

## SUPPLEMENTARY INFORMATION

### **Engineering of efficiency limiting free carriers and interfacial energy barrier for an enhancing piezoelectric generation**

Jung Inn Sohn,<sup>ad</sup> SeungNam Cha,<sup>\*ad</sup> Byong Gwon Song,<sup>ab</sup> Sanghyo Lee,<sup>b</sup> Seong Min Kim,<sup>a</sup>  
JiYeon Ku,<sup>a</sup> HyunJin Kim,<sup>a</sup> Young Jun Park,<sup>a</sup> Byoung Lyong Choi,<sup>a</sup> Zhong Lin Wang,<sup>c</sup> Jong  
Min Kim<sup>\*ad</sup> and Kinam Kim<sup>a</sup>

<sup>a</sup>Frontier Research Lab., Samsung Advanced Institute of Technology, Yongin, 449-712,  
Korea

<sup>b</sup>Department of Physics, Hanyang University, Seoul 133-791, Korea

<sup>c</sup>School of Materials Science and Engineering, Georgia Institute of Technology, Atlanta,  
Georgia 30332-0245, United States

<sup>d</sup>Department of Engineering Science, University of Oxford, Oxford OX1 3PJ, UK

\*To whom correspondence should be addressed. E-mail: seungnam.cha@eng.ox.ac.uk,  
jong.kim@eng.ox.ac.uk

### **The deposition of interlayers between an ITO electrode and piezoelectric semiconducting ZnO**

As a work function of the ITO film (4.8 eV) is higher than the electron affinity of ZnO (4.3 eV), a Schottky barrier is formed at the interface. For increasing more Schottky barrier height, we deposited 50 nm thick Au (with a work function of 5.1 eV) and Pt (with a work function of 5.7 eV) films on the ITO electrode using an electron-beam evaporator. For a MoO<sub>3</sub> interlayer, we used 50 nm thick MoO<sub>3</sub> films on ITO electrode and ZnO NWs, respectively using a thermal evaporation method. Our MoO<sub>3</sub> film has a work function of 5.7 eV.

### **Calculation of piezoelectric potential in ZnO NWs**

For the calculation of piezoelectric potential distributions as a function of donor concentrations, we assume that a ZnO NW has a cylindrical shape with a hexagonal cross section, 200 nm in diameter and 1 μm in length. The bottom of the ZnO NW was affixed to a substrate and electrically grounded because we consider that the ZnO NW is epitaxially grown along the c-axis on the substrate. A constant pressure of  $5 \times 10^7$  N/m<sup>2</sup> is exerted along the NW length on its tip surface and the resultant piezoelectric potential is calculated at the top of the NW as a function of donor concentrations ranging from  $10^{12}$  to  $5 \times 10^{17}$  cm<sup>-3</sup>. For the calculation of piezoelectric potential distributions as a function of the surface charge density, the NW is modeled as a cylinder oriented along the z-axis with the diameter of 200 nm and the length of 1 μm. We calculated piezoelectric potential distributions for the different surface charge density ranging from  $-3 \times 10^{-4}$  to  $-1 \times 10^{-3}$  C/m<sup>2</sup> under the same parameters by assuming that the entire NW surface is uniformly

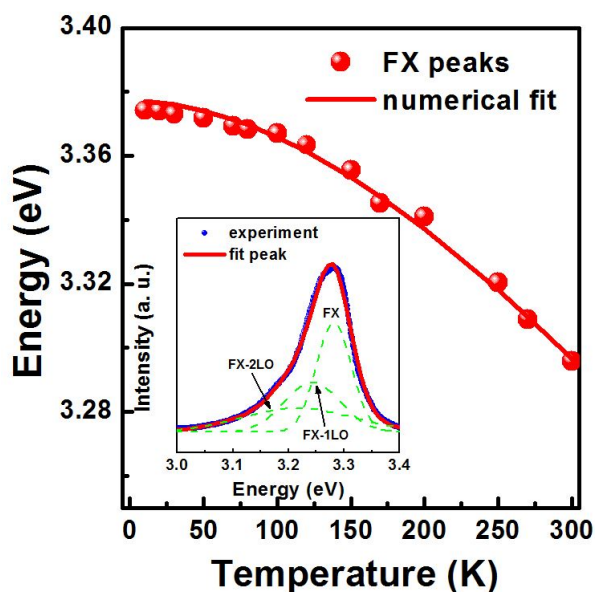


**Figure S1.** The temperature dependence of free exciton (FX) peak energy positions obtained from 25 mM Li-doped ZnO NWs in the range of 10 – 300 K. The solid line is the fitting curve by Varshni's formula. It can be seen that the FX peak shows a continuous redshift with increasing temperature. The experimental data are well fitted by the formula. This perfect match between the experimental data and the fitting curve further supports our assignment of PL peaks. (Inset) The shape of the room-temperature PL spectrum was fitted using Lorentzian functions, which are good approximation to determine the relative peak positions of FX and its longitudinal optical (LO) phonon replicas. The sum of the three Lorentzian curves (FX, FX-1LO, FX-2LO) is indicated by the solid curve (red).

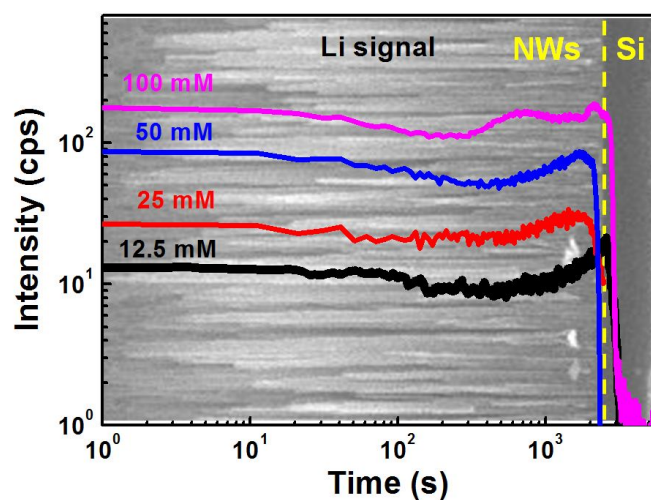


**Figure S2.** The Li signal SIMS depth profile of the Li-doped ZnO NWs, showing the spatial distribution and relative contents of Li atoms incorporated in NWs. We clearly observed the constant Li signal over the entire length of NWs for all samples doped with Li atoms regardless of Li concentrations, whereas no Li signal was detected from undoped ZnO NWs. Thus, this confirms the presence of Li incorporated uniformly in the NW and the signal relatively arises with increasing Li concentrations.

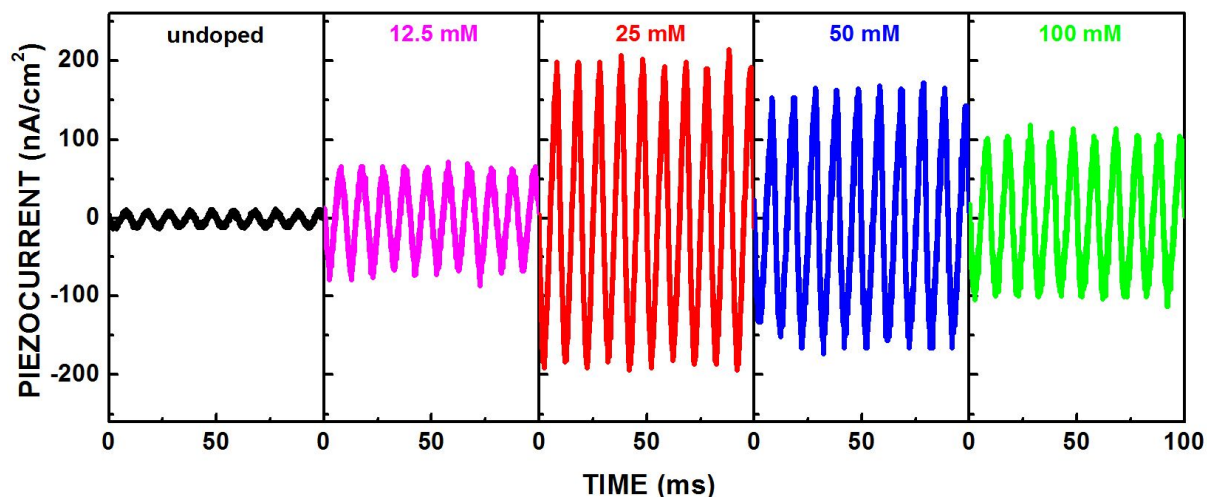


**Figure S3.** Piezoelectric output currents measured from SPENGs consisting of integrated Li-doped ZnO NWs with different donor concentrations. Akin to the tendency of the enhancement in the output piezopotential, the measured piezocurrent is significantly affected by donor concentrations due to the piezoelectric field screening. As expected, the piezocurrent of all devices is greatly increased after Li doping. Specifically, the average current density for 25 mM Li-doped ZnO NWs is estimated to be approximately 200 nA/cm<sup>2</sup>, which is over 21 times higher than that of undoped NWs.

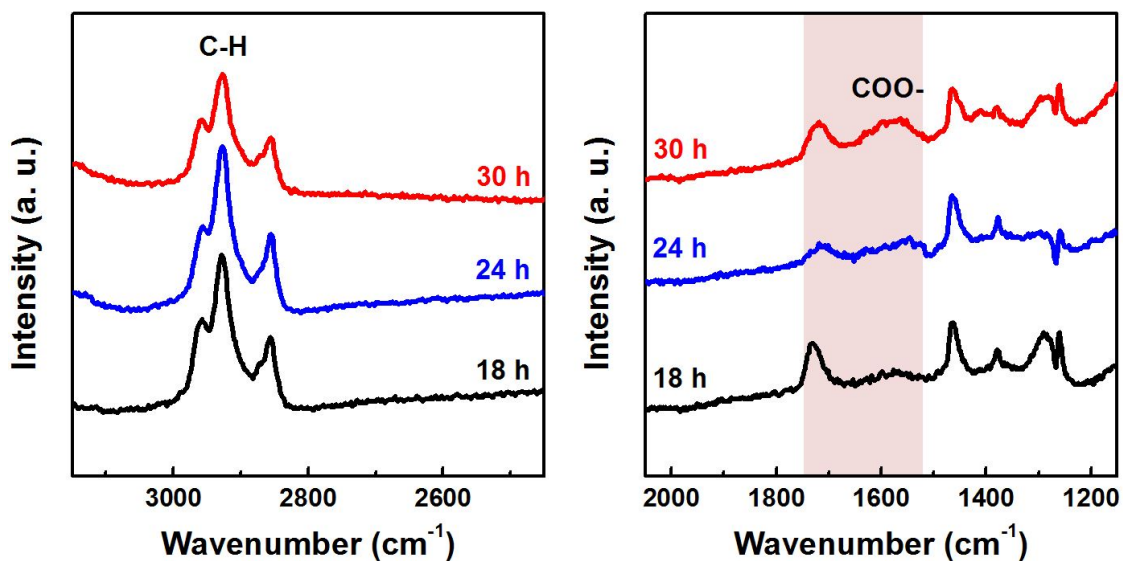


**Figure S4.** FT-IR spectra of oleic acid functionalized ZnO NWs for 18 h, 24 h, and 30 h, respectively. Generally, the intensity of FT-IR spectra for the surface-modified ZnO NWs is considerably weak due to the relatively small amounts of surface-anchored molecules. Nevertheless, we clearly observed a broad peak around  $1580\text{ cm}^{-1}$ , indicating COO- asymmetric stretching, and C-H stretching peaks in the range of  $2800 - 3000\text{ cm}^{-1}$ . In addition, the peak related to the carboxylate species becomes strong with increasing the functionalization time. These results provide the evidence that ZnO NW surface is successfully functionalized through the carboxylic group of the oleic acid.

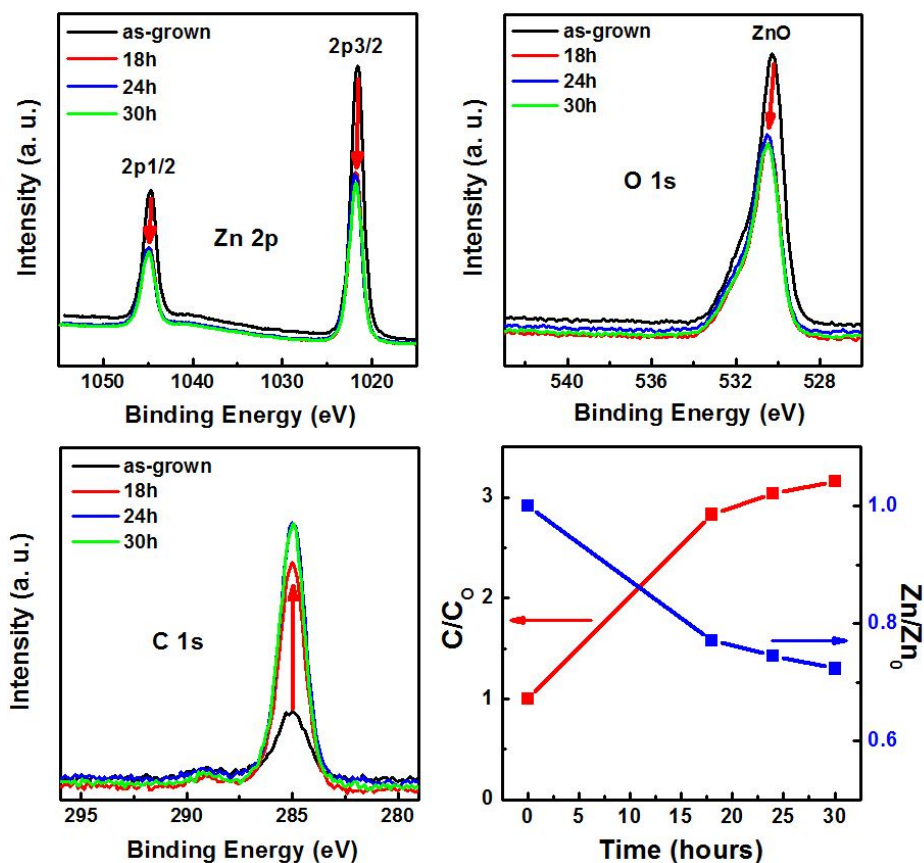


**Figure S5.** XPS spectra of surface-modified ZnO NWs as a function of the functionalization time. It is shown that as the functionalization time increases the intensity in the spectra of the Zn 2p and O 1s decreases, while the C 1s signal becomes strong with increasing time. This is because that the bare NW surface is completely exposed to the X-ray beam, while the functionalized surface is covered by the oleic acid molecules, giving the decreased photoelectron yield. These findings indicate that the ZnO NW surface was successfully modified with the oleic acid layer.

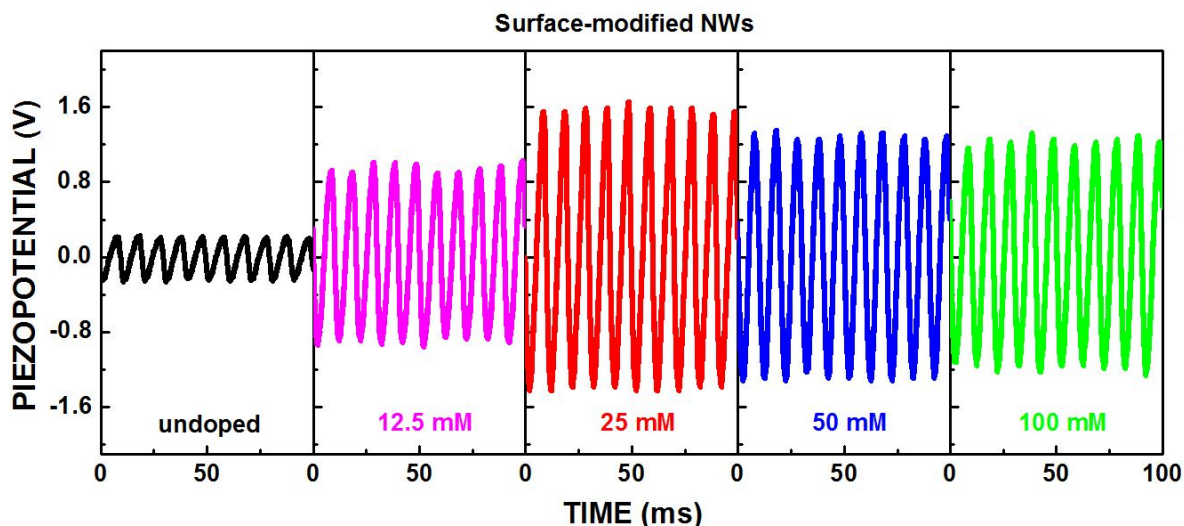


**Figure S6.** Piezoelectric output characteristics of SPENGs with surface-modified ZnO NWs. Specifically, taking into account the effect of donor concentrations on the piezoelectric potential, it has been shown that the presence of the negatively charged carboxylic group bonded on the ZnO NW surface, which results in the a depletion of electrons due to the repulsive force between the charged carboxylic group and electrons in NWs, significantly increases the output potential. In addition, there is a more effective and larger increase in output voltages for undoped and relatively low Li-doped samples as compared with for samples with relatively low donor concentrations. This result would be crucial in properly designing efficient nanogenerators with the high output.



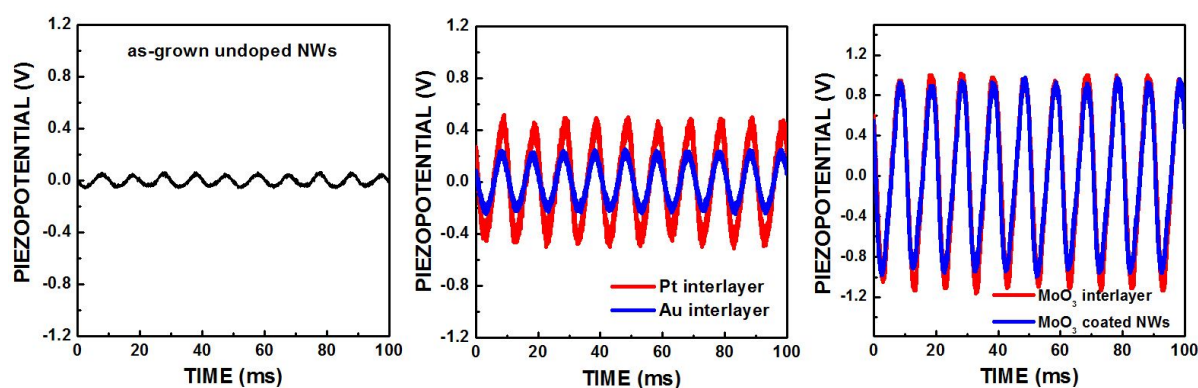


**Figure S7.** Piezoelectric performance of a SPENG with an interlayer. Noticeably, a considerable enhancement in piezoelectric output voltages was observed after the insertion of various interlayers such as Au, Pt, and MoO<sub>3</sub> with a larger work function than that of an ITO electrode. The incorporation of an interlayer with a high work function leads to the formation of a high Schottky barrier resulting in the decrease in leakage current through the MS interface. Interestingly, the insertion of a MoO<sub>3</sub> interlayer having a similar work function to Pt improved more the output voltages as compared to a Pt interlayer. In addition, there is a negligible change in piezopotential between SPENGs with a MoO<sub>3</sub> layer deposited on the electrode and a MoO<sub>3</sub> layer deposited on NWs. These results indicate that a MoO<sub>3</sub> interlayer with a high work function and deep conduction band minimum significantly enhances the performance of a SPENG due to the formation of an effective interfacial barrier to block electron transport through the interface.